INL/CON-21-62635-Revision-0

Creating Hydride Rim Structures in Zircaloy 4 Cladding Tubes to Mimic High Burnup

July 2021

David W Kamerman, David L Cottle, Arvin Burnell Cunningham, Austin C Matthews

Changing the World's Energy Future

INL is a U.S. Department of Energy National Laboratory operated by Battelle Energy Alliance, LLC

INL/CON-21-62635-Revision-0

Creating Hydride Rim Structures in Zircaloy 4 Cladding Tubes to Mimic High Burnup

David W Kamerman, David L Cottle, Arvin Burnell Cunningham, Austin C Matthews

July 2021

Idaho National Laboratory
Idaho Falls, Idaho 83415

http://www.inl.gov

Prepared for the
U.S. Department of Energy
Under DOE Idaho Operations Office
Contract DE-AC07-05ID14517

CREATING HYDRIDE RIM STRUCTURES IN ZIRCALOY 4 CLADDING TUBES TO MIMIC HIGH BURNUP

D.W. KAMERMAN, D.L. COTTLE, A.B. CUNNINGHAM, A.C. MATTHEWS
Idaho National Laboratory
1955 N Fremont Ave, Idaho Falls, ID 83415 – USA

ABSTRACT

During their long service in commercial light water reactors, zirconium alloy cladding tubes are subject to oxidation and subsequent hydrogen pickup which can degrade the materials' mechanical properties [1]. These degradations can lead to premature cladding ruptures during reactor power transients [2] as well as negatively impact the claddings post quench ductility following high-temperature steam oxidation in thermal-hydraulic transients [3]. Hydrogen has low solid solubility in zirconium and usually precipitates as brittle zirconium hydride platelets in the cladding metal matrix. Due to temperature-driven diffusion (Soret effect) and the grain texture of stress relieved zirconium metal tubes, these hydrides precipitate with a circumferential orientation near the outer surface of the cladding tubes forming a hydride rim which can serve as a site for crack initiation during circumferential 'hoop' loading of the cladding [4][5]. To better understand the effect of hydride rims on the fracture behavior of stress relieved zirconium alloy cladding tubes a procedure to produce these rim-like structures is being developed at Idaho National Laboratory (INL).

1 Introduction and Background

The conditions under which hydride rim structures form in commercial light water reactors are difficult to replicate in a laboratory setting. Figure 1 below shows examples of what these rim structures look like in actual high burnup cladding that was examined before transient testing [4]. Generating rim structures based on aqueous corrosion and Soret diffusion would require very long exposure times in autoclaves and would require a heat source inside the cladding tubes. Thus, an alternative method involving gaseous diffusion is being employed. Gaseous diffusion techniques for hydrogen charging have been employed previously by a variety of institutions and generally involve exposing a cleaned cladding tube to partial pressures of hydrogen gas (often in the form of H/Ar mixtures) at elevated temperatures between 300 C and 400 C [6][7]. Hydrogen charging apparatuses usually employ a flowing gas. Hellouin de Menibus et al developed a technique for forming a hydride blister on cladding tubes by bringing a cold finger into proximity with the cladding tube during hydrogen charging [8]. While hydride blisters are not the same feature as hydride rims their presence has been seen in high burnup cladding when heavy oxide formation and spallation occurs [9]. To create a hydride rim via gaseous diffusion, a supersaturation of dissolved hydrogen would need to be present near the outer surface of the cladding such that the driving force for precipitation is as high as possible. The rate of hydride precipitation in zirconium was studied by Marino et al [10] who proposed that the rate of hydride formation could be described by the following equation:

$$\frac{dC_{hydride}}{dt} = \alpha^2 (C_{disolved\ hydrogen} - TSS_p) \quad (1)$$

Where α is a kinetics parameter, C represents the concentration of hydrides and dissolved hydrogen respectively, and TSS_p is the terminal solid solubility (for precipitation) of hydrogen in zirconium. Both the kinetics parameter α and TSS_P follow Arrhenius relationships, which have been developed by Kammenzind [11] and McMinn [12] respectively. The activation energy for TSS_p is smaller however than α, thus as temperature increases, the driving force for precipitation will decrease for a given concentration of dissolved hydrogen. Thus, it is desired to conduct the hydrogen charging at as low of a temperature as possible to keep the rate of hydride formation as high as possible. The diffusion coefficient of hydrogen in zirconium also follows an Arrhenius relationship indicating that at high temperatures hydrogen will more readily diffuse through the thickness of the cladding further hindering rim formation [13]. However, a higher temperature will aid in the absorption of the hydrogen gas into the metal matrix, causing a faster hydrogen uptake and promoting supersaturation of the hydrogen in the metal.

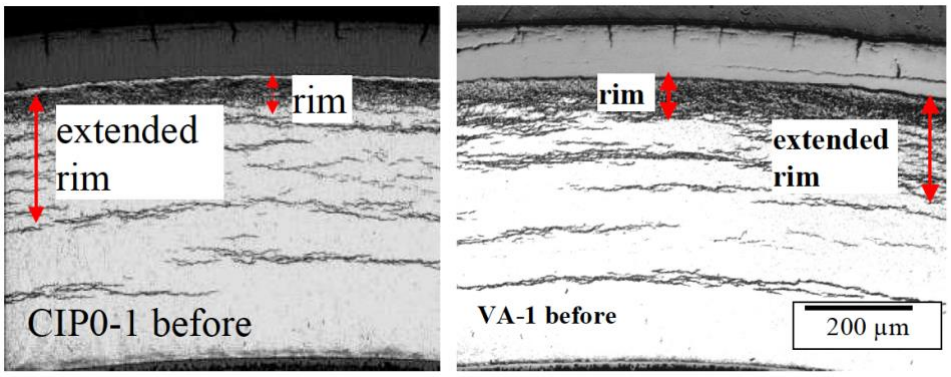

Figure 1) Hydride rims in cladding samples from CIP0-1 and VA-1 [4]

Apart from increasing the cladding temperature, the rate of hydrogen uptake can theoretically be increased by increasing the partial pressure of the hydrogen gas surrounding the cladding as done by Kudiiarov et al [14]. The hydrogen concentration in the metal is related to the square root of the partial gas pressure according to Sievert's law which is valid for zirconium metals and hydrogen [15]. Additionally, increasing the rate of hydrogen uptake can be achieved by increasing sample surface area via roughening of the surface which has been shown by Shimskey et al [16] as a successful way to form hydride rims in stress relieved zirconium metal cladding. An additional consideration in the preparation of zirconium metal cladding tubes for hydrogen charging is the presence of native oxide layers on the metal surface. Hydrogen is insoluble in Zirconium Oxide making the oxide layer an affect barrier to hydrogen uptake. Even after careful cleaning of the zirconium tubes, thin oxide layers (5-10 nm) will be present on the surface. To break down these oxide layers in a reasonable time interval, the cladding surface temperature must be elevated in an oxygen-deprived environment [17]. The minimum temperature (and time at temperature) for oxide layer breakdown depends on the starting condition of the oxide layer, the concentration of oxidizing agents in the gas surrounding the cladding, and the surface conditions of the oxide metal interface [18].

2 Materials and Methods

The hydrogen charging apparatus at INL consists of a 34 cm long tube furnace with a quartz tube insert that is connected to a vacuum pump as well as a bottle of 99.9% pure hydrogen gas. A single feed through in the quartz tube on the opposite end of the furnace allows a thermocouple to track the temperature in the center of the cladding tube when positioned in the furnace. Nuclear grade stress relieved Zircaloy-4 cladding tubes with standard 17x17 dimensions

(9.5 mm OD, 0.57 mm wall thickness) of 20 cm length are used in the present study. Charging cladding tubes of 20cm length will enable the generation of test specimens for more integral style mechanical tests such as burst testing [19], expansion due to compression testing [20], modified burst testing [21], and even integral transient testing [22] to take place. Well, variation in the hydrogen concentration and rim thickness is expected across the length of the cladding tube it is desired that the center 10 cm section of the charged tube be relatively uniform. Figure 2 below shows a diagram of the hydrogen charging apparatus at INL as well as a characterization of temperature uniformity across the length of the furnace at 290 C, 340 C, and 400 C. Temperature uniformity is important to maintaining uniform hydriding conditions. Minimal temperature variation is present in the center 20 cm of the furnace (+/- 10 C) and that this variation is reduced even further in the center 10 cm zone of the furnace (+/- 3C).

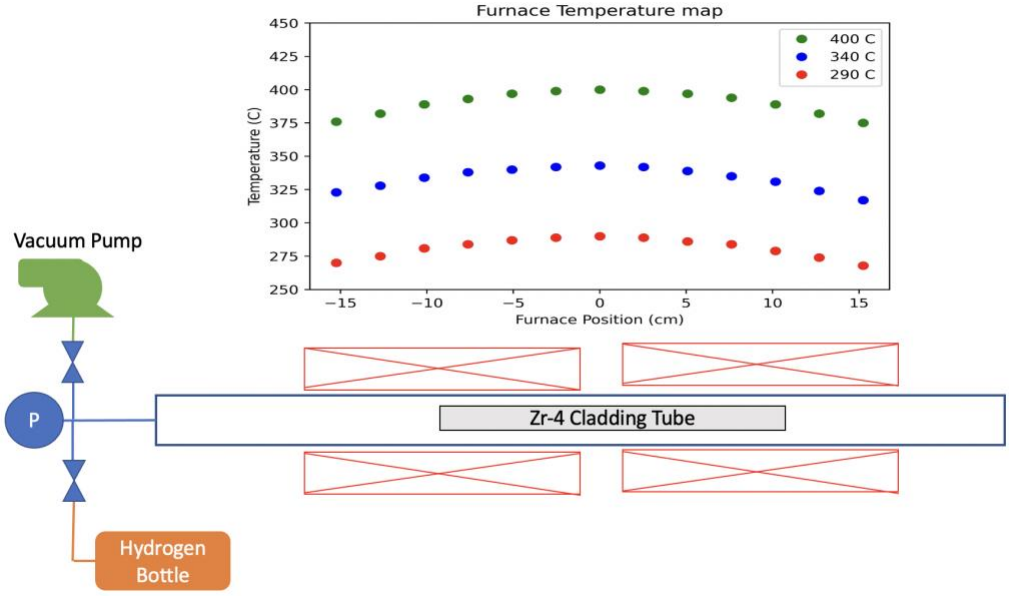

Figure 2) Diagram of Hydrogen Charging Station at INL along with Furnace Temperature Map

Contrary to most hydrogen charging apparatuses described in the literature, the charging station at INL uses a static charge of hydrogen in the quartz tube as opposed to a flowing gas. The chief advantage of this approach is the ability to monitor the pressure drop in the hydriding chamber and correlate this pressure drop to a known rate of hydrogen pickup in the cladding tube. A drawback of the static hydrogen charging approach is that as the hydrogen is absorbed into the cladding the hydrogen partial pressure driving further hydrogen uptake is reduced thus slowing the absorption rate. Hydriding should take place at a temperature sufficiently high to breakdown the native oxide layer on the cladding sample and provide sufficient energy to promote absorption of the hydrogen gas into the metal, however, increases in temperature above a certain threshold will prohibit rim formation as the driving force for diffusion will become greater than the driving force for precipitation. Given the desire to maintain low charging temperatures and use a static partial pressure of hydrogen gas, the chief means employed in the INL study for promoting hydride rim formation on the outer surface of the cladding tubes has been the careful preparation of inner and outer surfaces of the tubes before hydriding. It was postulated that smooth surfaces with thick oxide layers would prohibit hydrogen uptake while rough surfaces with very thin oxide layers would promote hydrogen uptake. It was desired to only create hydride rims on the outer surface of the cladding so efforts such as cleaning, hand sanding, and sandblasting were used on the outer surface of the cladding only. The inner surface was either left alone or an oxide layer was grown on the cladding surface by exposing the sample to air in a 400 C oven for 24 hours before

preparation of the outer surface and subsequent hydriding. Following sample preparation, the cladding would be loaded into the hydrogen charging furnace and the vacuum pump would be turned on for a duration of 10 minutes to 30 minutes until a vacuum pressure of 2e-9 psia was achieved in the system. Then an initial charge of hydrogen gas would be bled into the quartz tube. After the desired charge of hydrogen gas was added the valves to both the hydrogen bottle and vacuum pump would be closed and a 4 C/min ramp of the furnace would begin until the desired temperature was reached. Hydriding durations varied from 3 hours to over 120 hours depending on the rate of hydrogen uptake. Sixteen tests with 20 cm Zircaloy-4 tubes have been conducted to date with conditions shown in Table 1. Following the hydrogen charging, the cladding tubes were sectioned into analytical chemistry specimens, metallographic specimens, and mechanical test specimens following the sectioning diagram shown in Figure 3.

Table 1) Conditions of Hydrogen Charging Experiments

Test Number	Outer Surface Preparation	Inner Surface Preparation	Hydrogen Charge (psig)	Hydriding Temperature (C)
37	Clean	Clean	-7	290
38	Clean	Clean	-7	400
40	Clean	Clean	-7	400
41	Clean	Nothing	-7	290
43	Clean	Nothing	-7	350
44	Sand Blast	Nothing	-7	350
45	Sand Blast	Nothing	-7	290
46	Clean	Nothing	-7, & -2	350
47	Chemical Etch	Nothing	-7	350
48	Clean	Nothing	-7, & -2	290
49	Chemical Etch	Nothing	-7	290
50	Sandpaper	Oxidized	-7	290
55	Sandpaper	Oxidized	-4	290
57	Sandpaper	Oxidized	-4	290
543	Sandpaper	Oxidized	-4	290
563	Sandpaper	Oxidized	-4	290

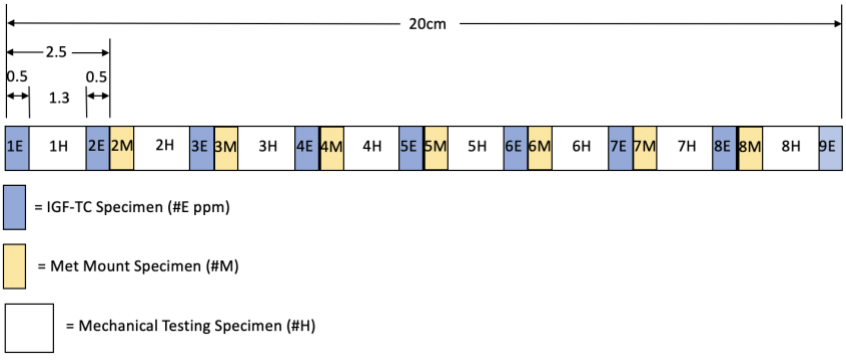

Figure 3) Cladding Tube Sectioning Diagram

3 Experiment Analysis

Analysis of the data from the hydriding runs was conducted to determine the rate of hydrogen uptake in the cladding tubes as well as the predicted final concentration of hydrogen in the cladding tube. To compare the uptake rates among various runs the rate of hydrogen uptake in the sample was determined by recording the time taken to observe a 4 psi pressure drop from the peak charging pressure, although not all of the 16 hydrogen charging experiments had this high of a pressure drop. In instances where a 4 psi pressure drop did not occur the hydrogen charging rate was determined to be the entire time, the furnace was at an elevated temperature. Any secondary additions of hydrogen gas (beyond the initial charge) during the hydrogen charging should take place quickly as the amount of hydrogen added is determined by a change in pressure during this time and it necessarily must be assumed that no hydrogen is absorbed in the cladding during that same time interval. This assumption is valid only when the rate of absorption is low and the time for the second hydrogen addition is short. Plots of temperature, pressure, and evaluated cladding hydrogen concentration during four of the sixteen hydrogen charging runs are shown below in Figure 4. It can be seen that the hydrogen gas pressure initially increases as the furnace heats up and then begins to decrease as hydrogen is absorbed into the cladding tube. Test 46 involved a secondary add of hydrogen gas. This addition occurred in about 13 seconds satisfying the conditions for secondary hydrogen adds.

To predict the presence and thickness of any hydrogen rims that may be forming during hydrogen charging a 1-D finite element diffusion model was employed to model hydrogen diffusion and hydride precipitation across the thickness of the cladding tube. The simulation was built using the BISON fuel performance code [23] with an integrated model for hydrogen diffusion and precipitation as developed and implemented by Courty [24] and Stafford [25]. These models for diffusion and precipitation of cladding hydrides were developed for use with a coupled cladding corrosion model, however, the settings of the hydrogen pickup function can be altered in the input file to allow for constant, time, or temperature-dependent hydrogen fluxes to be set as the surface boundary condition. The model requires the setting of a “hydride clamp” parameter which sets the maximum volume fraction of hydrides allowed in a given element. A “hydrogen clamp” of 0.1 (10% volume fraction) corresponds to a hydride concentration of ~1750 and is the recommended setting for LWR analysis, although this may not be appropriate for hydrogen charging in a gaseous environment. Nevertheless, the hydrogen clamp was set to 0.1 in all of the simulations presented in this work. Fifty-seven first-order linear elements were used each with a length of 10 μm to span the cladding thickness. An initial parametric evaluation was conducted to estimate the rim thickness when conducting hydrogen charging to 300 ppm, 500 ppm, 700 ppm, and 1000 ppm at 290 C, 340 C, and 400 C. A hydrogen absorption rate of 13.5 ppm/hr was chosen for the 290 C and 340 C simulations and a rate of 720 ppm/hr was chosen for the 400 C simulation. Through thickness concentrations of hydrogen from the parametric study is shown below in Figure 5. These results indicated that a hydriding temperature of 290 C would be most favorable for rim formation and that a minimum average cladding concentration of 500 ppm hydrogen would be required to form a rim. The model was also used to evaluate each of the 16 hydrogen charging experiments. Rim thickness was determined by the number of finite elements with hydride concentrations above 1250 ppm hydrogen.

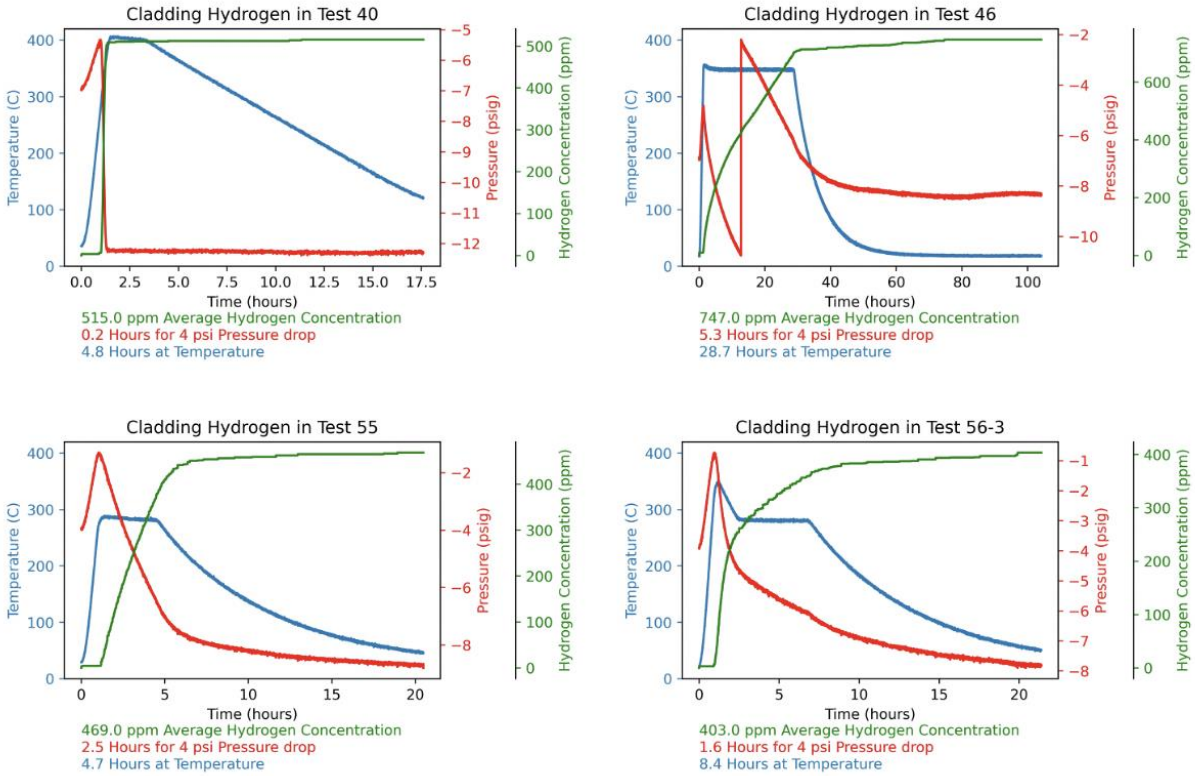

Figure 4) Temperature, Pressure, and Evaluated Hydrogen Concentration in Cladding Tube from Tests 40, 46, 55, and 56-3.

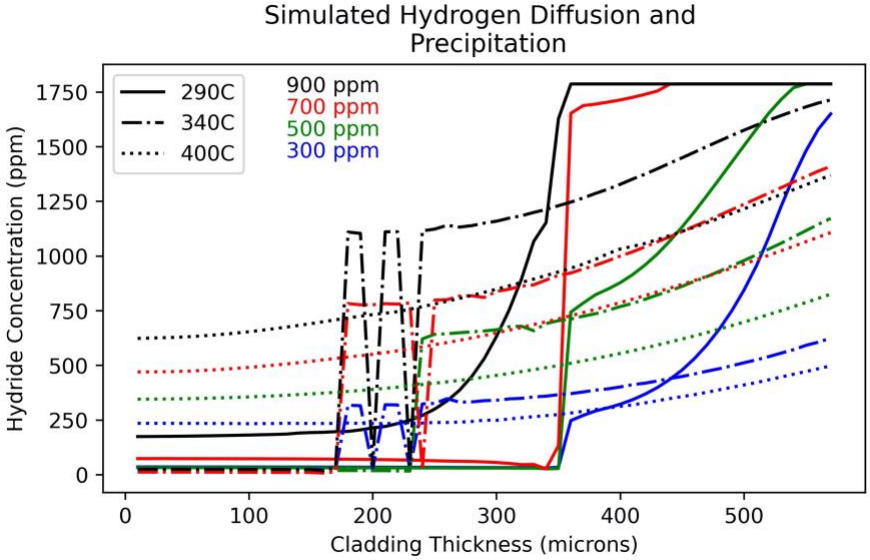

Figure 5) Results of Parametric FEA Study on Hydride Rim Formation

4 Results and Discussion

To date sixteen hydrogen charging experiments have taken place at 290 C, 350 C, and 400 C. The main results are shown in Figure 6. Twelve of the sixteen experiments have shown at least a 4psi pressure drop in the initial hydrogen charge and subsequent metallography and chemical analysis have confirmed the presence of circumferentially oriented hydride platelets in the cladding. Of the twelve experiments where the cladding experienced a meaningful hydrogen uptake, seven showed evidence of dense hydride rims in metallographic examinations. Of the seven tests that showed hydride rims, the hydride rim was exclusively present on the cladding outer surface in five of these experiments. All of the experiments which successfully formed hydride rims took place at either 290 C or 350 C and showed 4 psig pressure drops in under 24 hours with most successful cases showing these drops in under 10 hours. When considering the total time at temperature it appears that experiments lasting longer than 20-30 hours at 350 C and those lasting longer than 40-60 hours at 290 C will tend to result in uniform hydride formations with no observable hydride rims. While absorption happened even more rapidly at 400 C, it appears that rim formation is not possible at this temperature as neither of the two tests at this temperature showed evidence of hydride rim formation. Figure 6 below shows plots of all sixteen tests as functions of primary hydrogen charging temperature, time for 4 psi pressure drop, and total time at elevated temperature.

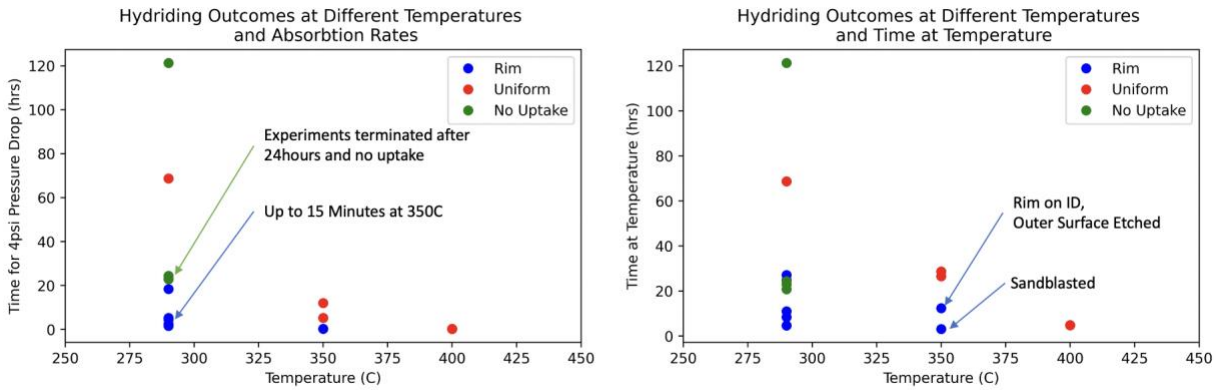

Figure 6) Results from 16 Hydrogen Charging Experiments at INL

Chemical determinations of cladding hydrogen content were conducted at a third-party laboratory using an inert gas fusion technique. Analytical chemistry measurements were not performed on every cladding tube due to cost and schedule constraints. A comparison of the chemically determined hydrogen concentrations across the length of the cladding with the evaluated tube average hydrogen concentrations based on observed pressure drop for tests 38, 50, and 55 is shown below in Figure 7. The chemical measurements show there is a significant variation in hydride concentration across the length of the cladding especially approaching the 5cm end regions where the temperature uniformity in the furnace begins to drop off. Across the center 10cm region the variation in cladding hydrogen concentration is less severe in most cases. The average hydrogen concentration determined by chemical analysis tended to vary by as much as 20% from the evaluated concentration based on observed pressure drop, although in some cases this variation was as small as 3%. The average concentration in the center of the charged tube was always higher than the evaluated concentration with a bias ranging from 7% to 22%.

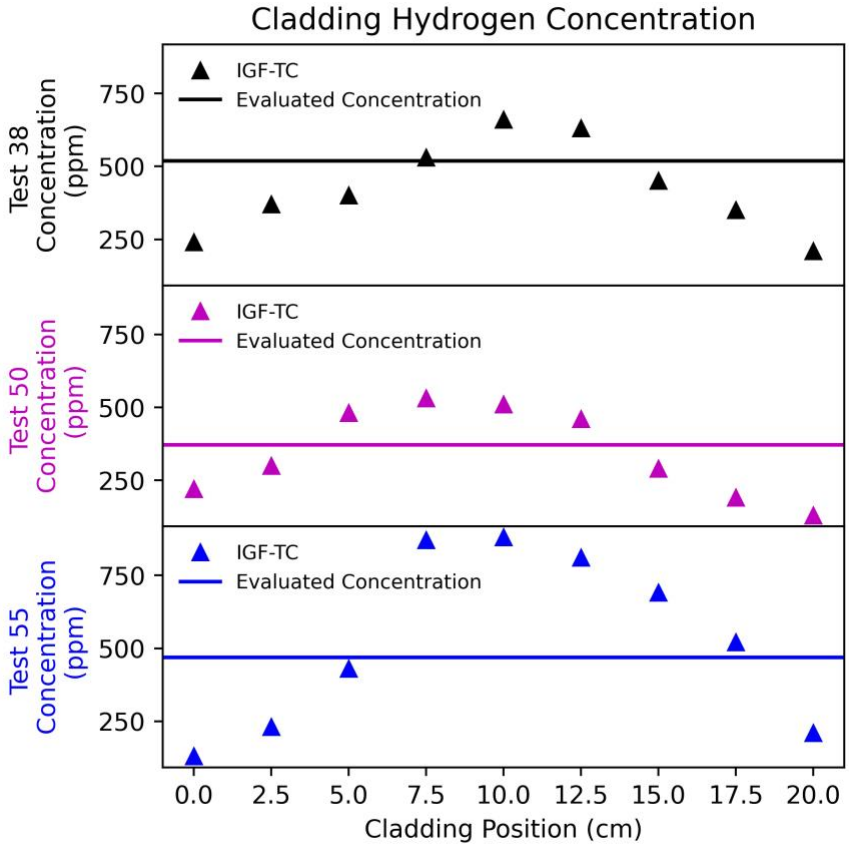

Figure 7) Comparison of Evaluated vs Measured Cladding Hydrogen Concentrations

Test 37 was the first to show clear evidence of rim formation, although this rim was present on both the outer and inner cladding surfaces. The surface preparation in test 37 involved a simple cleaning of the inner and outer surfaces and so this dual rim feature (shown in Figure 8) was to be expected. Test 44 was the next to show a successful rim formation, this time with much more prominence on the outer surface as the result of sandblasting the outer surface before hydrogen charging. Sandblasting however significantly altered the surface of the cladding and the rim feature that formed had more the appearance of a bulk uniform hydride than of a composite rim structure as seen in Figure 8. Chemical etching of the outer surface in tests 47 and 49 proved to inhibit hydrogen pickup on the outer surface and resulted in rim formation on the inner surface only on the former run and no hydrogen pickup in the latter run. Tests 50 and onward focused on a sample preparation technique that involved a pre-oxidation of the cladding tube to form oxide layers on both inner and outer surfaces. The outer oxide was then removed by hand sanding the outer surface which had the added benefit of slightly increasing the outer surface area but not altering it as dramatically as when sandblasting. All tests after 50 were performed with a principal charging temperature of 290 C, however, some tests were elevated to 350 C for a few minutes to promote native oxide layer breakdown and accelerate hydrogen uptake on the outer surface. Times at elevated temperature lasted up to 15 minutes before cooling to 290 C for up to 24 additional hours. The initial charge of hydrogen was also increased from -7 psig to -4 psig in later tests. Metallographic images from test 50, which is representative of almost all the later tests, is also shown below in Figure 8.

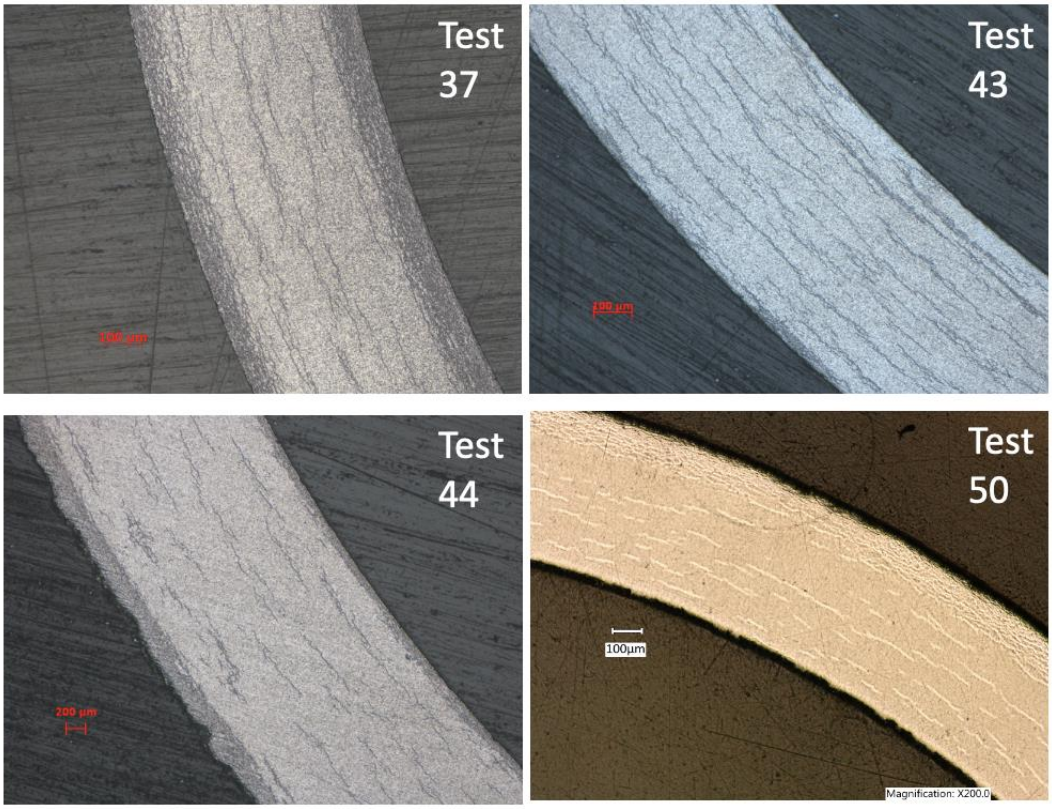

Figure 8) Metallographic images from Tests 37, 43, 44, and 50

Detailed rim thickness measurements were carried out on metallography samples from tests 50 and 55. Thirty-six measurements were made around the circumference of each of the eight metallography mounts. Variations in rim thickness could be rather significant around the circumference of the cladding as well as across the length. In test 50, the average rim thickness was 96.7 microns with standard deviations as high as 18 microns circumferentially and 23.7 microns across the length. In test 55 the average rim thickness was 52.3 microns with circumferential variation as high as 14 microns and axial variation of 8.8 microns. Comparison of measured rim thicknesses across the length of the cladding tubes is shown below in Figure 9 along with predicted rim thicknesses from the finite element model. The measured results differed substantially from the finite element model predictions of rim thicknesses of 50 and 110 microns for tests 50 and 55 respectively. In the case of test 50, the simulation under predicted the rim thickness but in test 55 the simulation over predicted the rim thickness. Additionally, in three tests (tests 43, 46, and 543) the finite element simulation predicted the formation of hydride rims however no rims could be clearly distinguished on the metallographic images. There were no cases where a rim was formed in the experimental condition but not predicted by the finite element model. A possible explanation for the poor performance of the finite element simulation may be that hydrogen diffusion is occurring more rapidly (or precipitation more slowly) in the actual experiments than as predicted in the simulation. More refined modelling efforts may take place as a part of future work on the effort to better address this discrepancy.

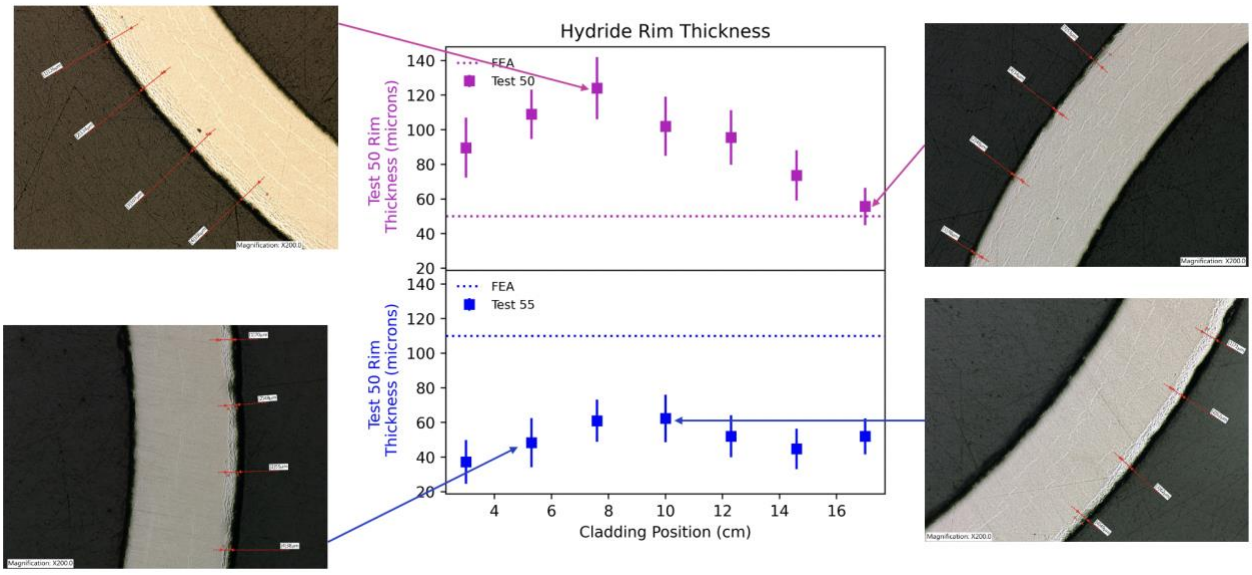

Figure 9) Measured Hydride Rim Thickness Variations in Tests 50 and 55

While the work is still preliminary it can be concluded that hydriding must take place at no greater then 350 C if a hydride rim is to be formed. Additionally, the rate of hydrogen uptake must be sufficiently high to create a super saturation of hydrogen in the outer surface of the cladding. It was determined that the rate of hydrogen uptake at a given temperature can be altered by manipulating the surface of the cladding where rough surfaces with small oxide layers such as those created from manual sanding work best to promote hydrogen absorption. To create hydride rim layers on only the outer surface of the cladding, it is necessary to prohibit hydrogen absorption on the inner surface of the cladding. This was achieved by growing an oxide layer on this surface by exposing it to air at elevated temperature (400 C).

5 Conclusions

A method to develop hydride rim features on stress relieved zirconium alloy cladding tubes used as nuclear fuel cladding in a hydrogen charging furnace similar to those seen in high burnup cladding is being developed at INL. Successful experiments to form these features involve pre-oxidizing the cladding tubes and then removal of the oxide layer from the outer surface of the cladding using a hand sanding process. The temperature ranges and absorption rates for hydrogen charging that favor rim formation was determined to be between 290 C and 340 C when significant hydrogen uptake occurs in less than 24 hours. The method of determining cladding average hydrogen concentration from pressure drop data during the experiment showed reasonable agreement with data from destructive chemical analysis. A finite element simulation that was developed to predict the conditions of rim formation proved useful in confirming the temperature range most favorable for rim formation but generally failed in predicting rim thicknesses within the range of what was observed experimentally. More work is needed to refine the finite element simulation as well as further refining the hydrogen charging procedure to produce more consistent and uniform results.

6 References

1 Allen T.R., Konings R.J.M., Motta A.T., “Corrosion of Zirconium Alloys” *Comprehensive Nuclear Materials* 5.03 (2012)

2 Fuketa T., “Transient Response of LWR Fuels” *Comprehensive Nuclear Materials* 2.22 (2012)

3 Nagase F., “Behavior of LWR Fuel During Loss-of-Coolant Accidents *Comprehensive Nuclear Materials* 2.23 (2012)

4 Georgenthum V., Sugiayam T., Udagawa Y., Fuketa T., Desquines J., “Fracture Mechanics Approach for Failure Mode Analysis in CABRI and NSRR RIA Tests” *2008 Water Reactor Fuel Performance Meeting*, Seoul Korea (2008)

5 Kim J.S., Kim H.A., Kang S.Y., Kim Y.S., “Effects of hydride rim on the ductility of Zircaloy-4 cladding” *Journal of Nuclear Materials* Vol 523 (2019)

6 Wang J.J., Wang H., Yan Y., *ORNL Interim Progress Report on Hydride Reorientation CIRFT Tests* ORNL/TM-2016/660 (2016)

7 Billone M.C., Burtseva T.A., Einziger R.E., “Ductile-to-Brittle transition temperature for high-burnup cladding alloys exposed to simulated drying-storage conditions” *Journal of Nuclear Materials* Vol. 443 (2013)

8 Hellouin de Menibus A., et al “Formation and Characterization of hydride blisters in Zircaloy-4 cladding tubes” *Journal of Nuclear Materials* Vol 449 (2014)

9 Hong K., Barber J.R., Touless M.D., Lu W., “Cracking and spalling of the oxide layer developed in high-burnup Zircaloy-4 cladding under normal operating conditions in a PWR” *Journal of Nuclear Materials* Vol 512 (2018)

10 Marino G.P., “Hydrogen Supercharging in Zircaloy” *Materials Science and Engineering* Vol. 7 (1971)

11 Kammenzind B.F., Franklin D.G., Peters H.R., Duffin W.J., “Hydrogen Pickup and Redistribution in Alpha-Annealed Zircaloy-4” *Eleventh Annual Zirconium in the Nuclear Industry* (1996)

12 McMinn A., Darby E.C., Schofield J.S., “The Terminal Solid Solubility of Hydrogen in Zirconium Alloys” *Twelfth Annual Zirconium in the Nuclear Industry* (2000)

13 Kearns J.J. “Diffusion coefficient of hydrogen in alpha zirconium, Zircaloy-2, and Zircaloy-4” *Journal of Nuclear Materials* Vol. 43 (1972)

14 Kudiiarov V., Sakvin I., Syrtanov M., Slesarenko I., Lider A., “Hydride Rim Formation in E110 Zirconium Alloy during Gas-Phase Hydrogenation” *Metals* (2020)

15 Puls M.P., *The Effect of Hydrogen and Hydrides on the Integrity of Zirconium Alloy Components,* Springer Oakville ON Canada, (2012)

16 Shimskey R., Hanson B., MacFarlan P., Optimization *of Hydride Rim Formation in Unirradiated Zr-4 Cladding,* PNNL-22835 (2013)

17 Cox B., “Mechanisms of Hydrogen Absorption by Zirconium Alloys*” Meeting of Materials Research Society* (1984)

18 Natesan K., Soppet W.K., *Hydrogen Effects on Air Oxidation of Zirlo Alloy,* NUREG/CR-6851 (2004)

19 Nagase F., Fuketa. T., “Investigation of Hydride Rim Effect on Failure of Zircaloy-4 Cladding with Tube Burst Test” *Journal of Nuclear Science and Technology* Vol 42 (2005)

20 Shinozaki T., Udagawa Y., Mihara T., Sugiyama T., Amaya M., “Improved-EDC tests on the Zircaloy-4 cladding tube with an outer surface pre-crack” *Journal of Nuclear Science and Technology* Vol 53 (2016)

21 Yueh K., Karlsson J., Stjarnstater J., Schrire D., Ledergerber G., Munoz-Reja C., Hallstadius L., “Fuel cladding behavior under rapid loading conditions” *Journal of Nuclear Materials* Vol 469 (2016)

22 Tomiyasu K., Sugiyama T., Fuketa R., “Influence of Cladding-Peripheral Hydride on Mechanical Fuel Failure under Reactivity-Initiated Accident Conditions” *Journal of Nuclear Science and Technology* Vol 44 (2007)
23 Williamson R.L., Hales J.D., Novascone S.R., Tonks M.R., Gaston D.R., Permann C.J., Andrs D., Martineau R.C., “Multidimensional multiphysics simulation of nuclear fuel behavior,” *Journal of Nuclear Materials*, Vol 423 (2012).
24 Courty O., Motta A., Hales J., “Modeling and simulation of hydrogen behavior in Zircaloy-4 fuel cladding” *Journal of Nuclear Materials* Vol 452 (2014)
25 Stafford D.S. “Multidimensional simulations of hydrides during fuel rod lifecycle” *Journal of Nuclear Materials* Vol 466 (2015)